A 3-D-Printed Dielectric Resonator for Triple-Mode Applications

Luke Robins, *Member, IEEE*, Chad Bartlett, *Member, IEEE*, Arash Arsanjani, *Member, IEEE*, Reinhard Teschl, *Member, IEEE*, Wolfgang Bösch, *Fellow, IEEE*, and Michael Höft, *Senior Member, IEEE*

***Abstract*— This work presents a novel 3-D-printed triple-mode dielectric resonator for microwave filter applications. The design demonstrates the use of an odd number of periodic rings placed along a dielectric combline resonator to create a miniaturized filter structure capable of creating a quasielliptic triple-mode filter response. A new approach suitable for 3-D-printing of the periodic rings is presented using support structures that take the form of struts. The resonator is fabricated using alumina with lithography-based ceramic manufacturing and housed in a compact single-cavity structure. The filter is designed for operation with a center frequency of 10.78 GHz, fractional bandwidth (FBW) of 2.13%, and a measured quality factor of approximately 1700.**

***Index Terms*— Additive manufacturing (AM), alumina, band-pass filter, dielectric resonator, stereolithography, triplet.**

I. Introduction

MICROWAVE filters are a critical part of modern telecommunications systems. In some circumstances, the technology chosen to implement the structure can result in bulky, heavy products or in formats that are difficult to integrate. Therefore, it is important to investigate miniaturization methods for these types of filters while working to maintain high-quality factors and dynamic filtering responses. Many approaches to miniaturization exist, such as the use of dielectric resonators, which reduce the structural size by compressing the electromagnetic fields [1], metamaterials [2], and multimode monoblock filters [3]. In a recent work on utilizing ceramic additive manufacturing (AM) for dielectric combline resonators [4], the quality factor performance of higher modes was increased and dual-mode operation was achieved through changes in the geometry. In this work, the concept of periodic changes in the geometry is expanded to triple-mode operations. A filter that utilizes the combination of the TM_{010} and the two orthogonal TE_{111} modes and operates at 10.78 GHz with a fractional bandwidth (FBW) of 2.13% is designed. It features increased distance to the next spurious mode while decreasing the material and weight at the same time, highlighting the flexibility in resonator design possibilities enabled through the use of ceramic stereolithography-based 3-D-printing.

Manuscript received 21 April 2023; revised 21 June 2023 and 15 August 2023; accepted 24 August 2023. Date of publication 19 September 2023; date of current version 8 November 2023. This work was supported by the European Union's Horizon 2020 Research and Innovation Program under the Marie Skłodowska-Curie Grant 811232-H2020-MSCA-ITN-2018. *(Corresponding author: Luke Robins.)*

Luke Robins, Arash Arsanjani, Reinhard Teschl, and Wolfgang Bösch are with the Institute of Microwave and Photonic Engineering, Graz University of Technology, 8010 Graz, Austria (e-mail: lrobins.p@gmail.com).

Chad Bartlett and Michael Höft are with the Department of Electrical and Information Engineering, Kiel University, 24143 Kiel, Germany.

Color versions of one or more figures in this letter are available at https://doi.org/10.1109/LMWT.2023.3311812.

Digital Object Identifier 10.1109/LMWT.2023.3311812

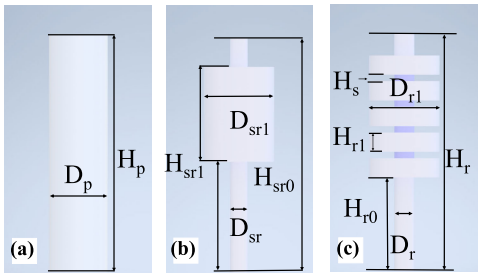

Fig. 1. Alumina ($\varepsilon_r = 9.5$ and $\tan\delta = 8{\cdot}10^{-5}$ [6]) resonator comparison: (a) post, (b) solid-ring, and (c) five-ring.

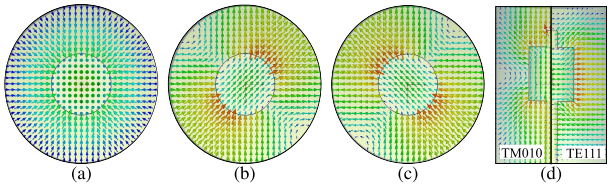

Fig. 2. Solid-ring E-field distributions middle cut. (a) TM_{010}. (b) TE_{111}. (c) $TE_{111\perp}$. (d) Side on view.

II. Triple-Mode Resonator Design

To demonstrate the build-up of the 3-D-printable resonator structure, a progression of the resonators is presented in Fig. 1. The most basic resonator configuration, consisting of a dielectric post placed in a cylindrical cavity, is shown in Fig. 1(a). The first four modes in this configuration are: TM_{010}, TM_{011}, TE_{111}, and TE_{112}. It is important to mention that these modes are not purely TM or TE due to the asymmetric placement of the resonator. However, the respective longitudinal field components are small. The addition of a solid ring (SR) on the post, as demonstrated in Fig. 1(b), can influence the positions of these modes relative to each other. The simulated field concentrations of the first two modes are illustrated in Fig. 2. From these, it can be observed that the TM mode has more field concentrated at the center of the cavity along the central post, while the TE mode is most concentrated near the outside edge of the introduced ring. These areas of field concentration can be exploited to, somewhat independently, shift the resonant frequency of the TM_{010} and TE_{111} modes, allowing the modes to be close enough together to be useful in a dual-mode configuration. Additionally, the TE_{111} has an

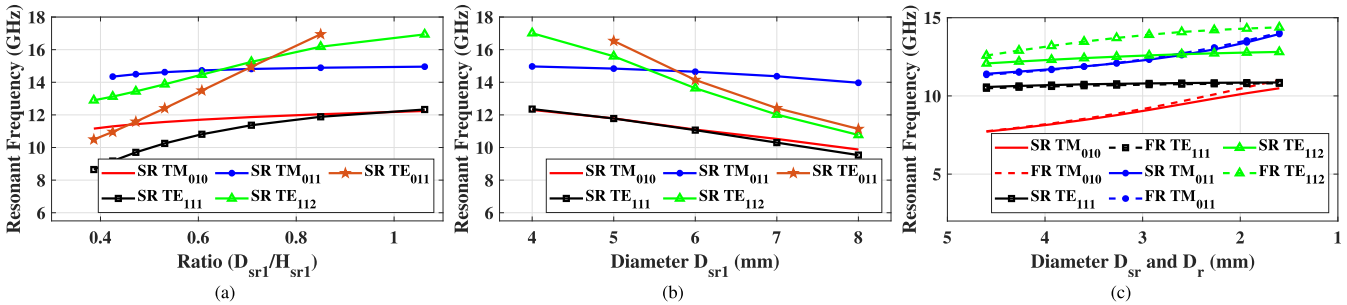

Fig. 3. Resonant frequency study for the SR and FR resonators, demonstrating the (a) triple-mode operation ratio while keeping a fixed height (H_{sr1} = 4.25 mm), (b) mode separation improvement with a fixed ratio (D_{sr1}/H_{sr1}) = 1, and (c) further mode separation using the FR resonator and sweeping the central post diameter with (D_{sr1} = D_{r1} = 5.6 mm).

identical orthogonal mode at the same resonant frequency [see Fig. 2(b) and (c)], and, therefore, a triple-mode implementation is possible. The effect of the ratio of ring height (H_{sr1}) to the outside diameter (D_{sr1}) is shown in Fig. 3(a). Interestingly, for the desired triple-mode operation point, the optimal ratio was found to be approximately 1. Parameter sweeps with this ratio fixed are shown in Fig. 3(b). Keeping the outside diameter of the SR fixed while sweeping the diameter of the central post (D_{sr}) is demonstrated in Fig. 3(c). These results demonstrated that the resonator can be optimized for both triple-mode operations and situated at a point where the distance to the next mode is a maximum, ultimately moving the TE_{111} away from the spurious TM_{011} and TE_{112} modes. Similar results can be achieved using a five-ring (FR) structure as shown in Fig. 1(c). A comparison of the respective shifts in resonant frequency, between SR and FR, can be seen in Fig. 3(c) and it highlights that the TE_{112} mode is shifted to higher frequencies when using the FR profile and gives approximately 60% (1 GHz) of additional separation to the desired modes.

III. Fabrication Considerations

Fabrication of the FR configuration would require approximately 22% less material and result in an 18% lighter resonator when compared to the SR resonator. Due to these advantages and the fact that the FR resonator has a higher degree of complexity, lithography-based 3-D-printing was chosen for fabrication. Using the principles outlined previously, a triple-mode resonator specified for 10.8-GHz operation was designed for fabrication. The model of the FR resonator is depicted in Fig. 1(c), where the dimensions are given as: H_{r0} = 5.62, H_{r1} = 1.5, H_r = 18.6, D_r = 1.6, D_{r1} = 5.6, and H_s = 0.5 (mm).

The resonators were fabricated using a Lithoz CeraFab 7500 printer, with an XY resolution of 40 μm and a printing-layer height of 50 μm. Multiple fabrication rounds were required to enable successful printing. The large difference between the central post and outside ring radius created overhangs too large to be easily printed without support. The transition areas from the post to the ring were prone to breakages during printing due to sheer stress.

To overcome this, supporting struts were introduced in between the rings as shown in Fig. 4. However, it should be noted that the addition of material can cause the TM modes to shift to lower frequencies, and therefore, keeping the struts as thin as possible was critical for the design to succeed. The final strut-adapted resonator design is shown in Fig. 4 with the following dimensions: H_{r0} = 9, H_{r1} = 1, H_r = 18.51, D_p = 1.6, D_r = 6.05, H_s = 0.5, R = 1, S_t = 0.12 (mm), and θ = 30°. The resonators have a simulated Q_u of approximately 11 000 in a copper cavity and 6000 in brass.

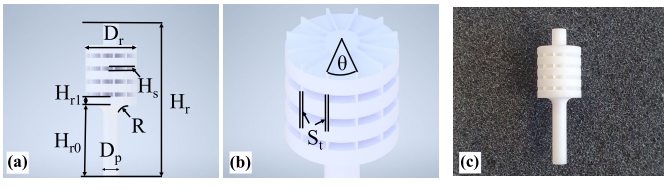

Fig. 4. Modified triple-mode resonator for printing. (a) Side view. (b) Perspective view. (c) Fabricated resonator.

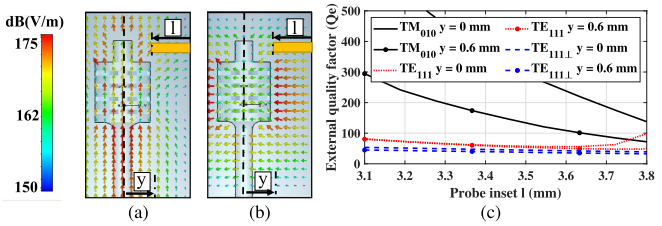

Fig. 5. Input coupling: (a) TM_{010}, (b) TE_{111}, and (c) simulated results.

IV. TM_{010} and TE_{111} Triple-Mode Filter

A third-order filter centered at 10.78 GHz with a return loss of 20 dB and an FBW of 2.13% was designed to verify the resonator concept and show an application of dynamic alumina-based 3-D-printing. The triplet uses a cylindrical cavity with a radius of 7.5 mm and a height of 21.8 mm and encompasses the 3-D-printed resonator specified in Section III. SMA probes were chosen as a simple approach to feeding, where the input coupling can be controlled by the length of the probe into the cavity. Horizontal placement of the probes was used as more space was available on each wall to accommodate both feeds for the triplet case. The probe feeding provides a challenge, as in this case, the TM_{010} and TE_{111} electric fields are almost entirely orthogonal to each other. The field configurations are shown in Fig. 5(a) and (b), highlighting a small area toward the top of the resonator where some of the electric field components are oriented horizontally

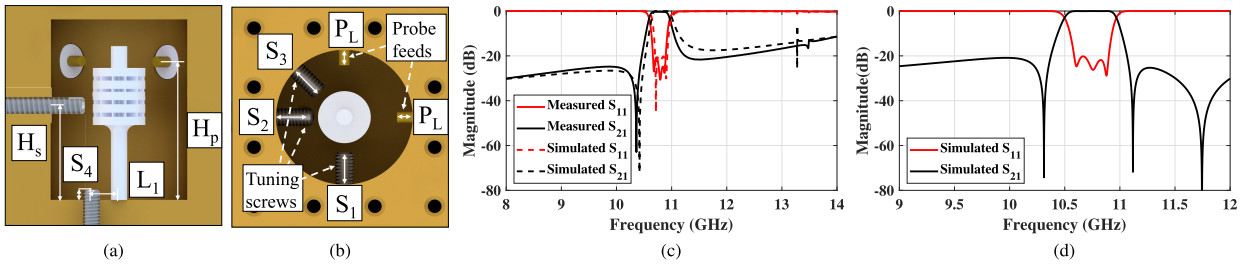

(a) (b) (c) (d)

Fig. 6. Designed triple-mode filter: (a) side view, (b) top view, (c) simulated and measured performance, and (d) alternate zero configuration.

for both modes. Placing the feeds at this position enables the simultaneous excitation of both modes. Fig. 5(c) shows the feasible input coupling achieved by varying the probe depth. The coupling can be further increased by a deliberate misalignment of the resonator with respect to the center of the cavity, as further demonstrated in Fig. 5(c), allowing for wider bandwidths and more gradual changes in regard to the input coupling.

To achieve triple-mode operation, the ports were placed at 90° relative to one another. A metallic screw was placed at 45° between the ports to excite both orthogonal TE_{111} modes and a metallic screw controlling TM_{010} was placed next to the resonator on the floor of the cavity. The screws are positioned close to the maximum electric field of the respective mode for the most impact. Two additional screws for each TE_{111} mode were included to allow for the tuning of each. The final filter responses and layout are provided in Fig. 6. Extraction of the exact coupling parameters in this triple-mode configuration is difficult due to innate parasitic and loading effects. Therefore, a simplified analogous transversal coupling matrix, which excludes the cross-coupling, is included to aid the initial filter design: MS1 = 0.59, M1L = 0.54, MS2 = 0.59, M2L = 0.54, MS3 = −0.81, M3L = 0.83, M11 = −1.6, M22 = 1.54, M33 = −0.135, and MSL = −0.039. The dimensions are given as: $P_L = 3.7$, $S_1 = 1.1$, $S_2 = 0.8$, $S_3 = 1.83$, $S_4 = 3.35$, $L_1 = 4.5$, $H_p = 11.4$, and $H_s = 9$ (mm).

The transmission zero (TZ) appearing below the passband is generated by the relationships between the input coupling to each mode with the source to $TE_{111\perp}$ having the opposite phase. In this case, the TZ position can be moved by keeping coupling into mode $TE_{111\perp}$ fixed and adjusting the coupling of TM_{010} and TE_{111}. As the coupling into TM_{010} is decreased and into TE_{111} is increased, the TZ moves downward away from the passband. The selected probe-feeding setup limits the flexibility in positioning the TZs, as changes in input coupling influence at least two of the modes at a time. There is, however, a way to keep the TZ below the passband and create an additional TZ above the passband; this is done by reducing the source-to-load coupling. This can be achieved by rotating one of the inputs by 25° clockwise from the position in Fig. 6(b), thus reducing the coupling between the ports. While the input coupling of the TM mode is independent of the rotation of the feeds, the coupling for the two TE modes changes based on the rotation of the feeding. This allows the response illustrated in Fig. 6(d), whereby the second TZ above the passband is caused by the higher-order TE_{112} mode interacting with the TE_{111} which bypasses the resonator. The simplified analogous transversal coupling matrix: MS1 = 0.52, M1L = 0.41, MS2 = 0.51, M2L = 0.52, MS3 = −0.87, M3L = 0.83, M11 = −1.5, M22 = 1.43, M33 = −0.17, and MSL = −0.017.

TABLE I
COMPARISON TO RECENT WORKS ON THE DIELECTRIC RESONATOR AND CERAMIC 3-D-PRINTED FILTERS

Ref.	f_0	FBW	Mode	Q_u	Volume*/λ_0^3
2017 [7]	8.3	1.25%	Single	600	0.031
2018 [5]	1.505	1%	Triple	5120**/4840**	0.007†
2022 [3]	6	4.64%	Dual	840	0.1276
2022 [4]	13.8	0.3%	Dual	3700**/1800	0.114†
2022 [9]	6.1	44%	Single	1000	0.124†
2022 [10]	14.125	5.3%	Dual	5600**/4000	0.145
2023 [11]	2.93	2.8%	Single	1000	0.00725†
T.W.	10.78	2.13%	Triple	3600**/1700	0.062†

*Per electric resonator,**simulated, †excl. housing

V. FABRICATION AND MEASUREMENT

The designed resonator and filter cavity were fabricated using Lithalox 350 and brass, respectively, with a resonator shown in Fig. 4(c). The resonator was glued to the bottom lid by hand using superglue and, as such, makes achieving an exact alignment difficult, leading to slight shifting in frequency and quality factor degradation. However, this simple process is accurate enough for a proof-of-concept filter and allows for the verification of the performance of the 3-D-printed resonator. The measured filter performance is compared to the simulated S-parameter in Fig. 6(c) and largely matches that of the simulation, aside from a 40-MHz shift. The extracted quality factor is approximately 1700, while the simulated value is in the range of approximately 3600. These deviations are attributed to the manual assembly process and additional losses introduced by the superglue and the tuning screws. Table I provides a comparison of this work to recent 3-D-printed filters and demonstrates the overall compactness while still maintaining quality factor performance.

VI. CONCLUSION

This work introduces a novel 3-D-printed triple-mode dielectric resonator that enables the use of the TM_{010} and the two orthogonal TE_{111} modes together in a triplet implementation. Additionally, the work presents a thin strut-like support geometry to enable the printing of alternating ring-type structures. The resonator was fabricated and demonstrated for a triplet filter implementation operating at 10.78 GHz, highlighting potential applications of 3-D-printed ceramic resonator structures.

REFERENCES

[1] V. Nocella, L. Pelliccia, C. Tomassoni, and R. Sorrentino, "Miniaturized dual-band waveguide filter using TM dielectric-loaded dual-mode cavities," *IEEE Microw. Wireless Compon. Lett.*, vol. 26, no. 5, pp. 310–312, May 2016, doi: 10.1109/LMWC.2016.2549181.

[2] A. Arsanjani, C. Bartlett, L. Robins, R. Teschl, W. Bösch, and M. Höft, "Metasurfaces for filter miniaturization and out-of-band rejection improvement," *IEEE Microw. Wireless Technol. Lett.*, vol. 33, no. 3, pp. 271–274, Mar. 2023, doi: 10.1109/LMWT.2022.3221467.

[3] D. Miek et al., "Ceramic additive manufactured monolithic X-shaped TM dual-mode filter," *IEEE J. Microw.*, vol. 2, no. 3, pp. 496–506, Jul. 2022, doi: 10.1109/JMW.2022.3167250.

[4] L. Robins et al., "3D-printed dielectric resonators for quasi-TE112 mode singlets, doublets and dual-mode filters," *IEEE Access*, vol. 10, pp. 130326–130338, 2022, doi: 10.1109/ACCESS.2022.3228764.

[5] X. X. Yuan, L.-H. Zhou, and J.-X. Chen, "Triple-mode bandpass filter based on silver-loaded ring-shaped dielectric resonator," *IEEE Microw. Wireless Compon. Lett.*, vol. 28, no. 9, pp. 789–791, Sep. 2018, doi: 10.1109/LMWC.2018.2853568.

[6] Lithoz. *Materialübersicht LCM-Technologie*. Accessed: Jul. 25, 2022. [Online]. Available: https://lithoz.com/wp-content/uploads/2022/04/LITHOZMaterialfolder DE web.pdf

[7] C. Carceller, F. Gentili, D. Reichartzeder, W. Bösch, and M. Schwentenwein, "Development of monoblock TM dielectric resonator filters with additive manufacturing," *IET Microw., Antennas Propag.*, vol. 11, no. 14, pp. 1992–1996, Nov. 2017, doi: 10.1049/iet-map.2016.1051.

[8] A. Perigaud, O. Tantot, N. Delhote, S. Verdeyme, S. Bila, and D. Baillargeat, "Bandpass filter based on skeleton-like monobloc dielectric pucks made by additive manufacturing," in *Proc. 48th Eur. Microw. Conf. (EuMC)*, Sep. 2018, pp. 296–299, doi: 10.23919/EuMC.2018.8541710.

[9] A. Widaa, F. Cacciamani, L. Pelliccia, C. Tomassoni, V. T. di Crestvolant, and M. Höft, "Compact ultra-wideband bandpass filter using additively manufactured TM-mode dielectric resonators," in *Proc. 52nd Eur. Microw. Conf. (EuMC)*, Sep. 2022, pp. 115–118, doi: 10.23919/EuMC54642.2022.9924504.

[10] E. López-Oliver, C. Tomassoni, F. Cacciamani, L. Pelliccia, and V. T. D. Crestvolant, "Bandpass filter based on 3-D-printed ceramic resonators," in *Proc. 24th Int. Microw. Radar Conf. (MIKON)*, Sep. 2022, pp. 1–5, doi: 10.23919/MIKON54314.2022.9924680.

[11] A. Widaa, C. Bartlett, and M. Höft, "Design of compact quasi-elliptic bandpass filters based on coaxial inset resonators," *IEEE Access*, vol. 11, pp. 18739–18749, 2023, doi: 10.1109/ACCESS.2023.3247137.